IEEE Access
Multidisciplinary | Rapid Review | Open Access Journal

Received August 11, 2020, accepted August 28, 2020, date of publication August 31, 2020, date of current version September 15, 2020.

Digital Object Identifier 10.1109/ACCESS.2020.3020646

Flexibility Robust Optimal Operation Strategy for Cross-Regional Interconnected Power Under Load-Source Coordination

XIAOZHU LI[1], WEIQING WANG[1], HAIYUN WANG[1], JIAHUI WU[1], AND QIDAN XU[2]

[1]Engineering Research Center for Renewable Energy Generation and Grid Connection Technology, Ministry of Education, Xinjiang University, Ürümqi 830047, China

[2]State Grid Xinjiang Economic Research Institute, Ürümqi 830000, China

Corresponding author: Weiqing Wang (wangweiqing1230@126.com)

This work was supported in part by the National Natural Science Foundation of China under Grant 51667020, in part by the Opening of Laboratory in Xinjiang Autonomous Region under Grant 2018D04005, and in part by the Key Natural Science Projects of Universities under Grant XJEDU2019I009.

ABSTRACT Ultra High Voltage (UHV) transmission technology is the main regional power interconnection method in China. In addition, renewable energy sources (RES) in China are characterized by centralized distribution. In view of the cross-regional flexible scheduling of large-scale grid-connected RES, we build a day-ahead optimization model which considers the generation economy and robustness of transmission for each regional grid. The model considers the spatial clustering effect of RES and loads, uses robust optimization theory to construct uncertainty sets, and introduces uncertain spatial constraint parameters to compensate for the insufficiency of traditional robust optimization. Furthermore, a co-evolutionary algorithm filter-based is proposed to solve above the mixed-integer non-convex nonlinear programming model. Taking the modified IEEE-39 nodes as an example, the results show that the system cost can be reduced by 21.9% by selecting the confidence probability of uncertain variables of both load and source under stable operation, while the prediction accuracy has a significant impact on the system cost when the confidence probability is smaller, and a better operation scheme can be obtained by increasing the space constraint parameters. Finally, the feasibility of the proposed model and algorithm are verified on the Hami power grid in Xinjiang, China.

INDEX TERMS Co-evolutionary algorithm, filter technology, flexible scheduling, interconnected power systems, robust optimization.

I. INTRODUCTION

Ultra High Voltage (UHV) transmission technology has become the main physical method of regional power interconnection in China [1]. The cross-regional interconnected power grid (CRIG) [2], which has been a key driver of Chinese development, has evolved through a complex and lengthy process that has been influenced by numerous factors. Using UHV transmission, the CRIG system can effectively alleviate imbalances between the power supply and demand across regions that result from large-scale and long-distance transmission, thus promoting the rapid development of renewable energy sources (RES). However, the bilateral instability caused by large-scale grid-connected RES and increasing loads inhibit the CRIG's capability to respond flexibly to power fluctuations [3]. Therefore, considering the uncertainty of both power generation and loads, flexible dispatching among regions using existing resources has important practical significance for balancing the power supply and ensuring the sustainable development of power interconnection.

In recent years, many studies have focused on dispatching modes and energy management models of CRIGs. These studies have laid a theoretical foundation for our research but there exist many problems that have not been fully considered. For example, a decentralized scheduling method has been proposed [4] that takes into account the cross-regional tie-line transaction plan. Although this decentralized scheduling method overcame the shortcomings of traditional centralized scheduling, but it did not consider the fluctuation of loads

The associate editor coordinating the review of this manuscript and approving it for publication was Amjad Anvari-Moghaddam.

This work is licensed under a Creative Commons Attribution 4.0 License. For more information, see https://creativecommons.org/licenses/by/4.0/

and RES. In [5], the uncertainty of wind power and photovoltaic output were considered for a proposed decentralized robust dispatch scheme for multi-area power systems, but the load uncertainties were ignored and the model could not balance economy and robustness flexibly, so the results were too conservative. In [6] a stochastic chance-constrained programming scheduling model was proposed, which considers the uncertainties of both sources and loads. However, the security and stability of the system were not considered, and the relationship between uncertainties' and constraints' confidence levels could not be determined. In [7], a coordinated optimal dispatching model that benefits through integrated energy interconnection among regions was proposed. The above-mentioned methods not only fail to respond flexibly to source and load fluctuations, but are also unable to balance economy and robustness reasonably. At the same time, the threshold effect with non-convex characteristics of thermal units has not been considered in [7]–[10], so the local optimal solutions of the non-convex optimization problem are no longer globally optimal solutions, which are more difficult to attain than in convex problems.

Moreover, the multiple uncertainties from both the generation and the consumption side (such as wind generator and PV output, load, etc.) are still the main challenges that CRIGs face during operation. The methods to describe these uncertainties can be summarized as standby setting methods [11] and stochastic programming methods [12]. The above two fields have witnessed continuous exploration by many scholars, resulting in solutions based on fuzzification [13], scenario analysis [14], spectrum analysis [15], point estimation [16] and stochastic chance constrained programming [17], whose effectiveness and practicability are being continuously improved. However, there still exist many problems, such as the subjective selection of membership functions, the need for a large amount of sample data, the limited number of scenarios for which results are obtained, the complexity of multi-scene description uncertainty, and others, and it is difficult to ensure the efficiency and accuracy of solutions. The theoretical framework of robust economic dispatch of power systems is proposed from the perspective of robust optimization, which opens up a new idea for power uncertainty modeling [18]–[20].

Most robust optimization problems can be formulated as max-min problems, which is the optimal solution of the system in the worst case in order to ensure the robustness of the system. However, in many cases the extreme situation will not occur, or the probability of occurrence is close to 0. Under such circumstances traditional robust optimization ignores economic aspects while improving the robustness of the system, which makes the dispatching results too conservative. The selection of the worst case considered for the optimization problem, adjusting the boundaries of the robust set reasonably, and balancing economic and robustness aspects scientifically are problems that still require further study.

Furthermore, to improve the flexibility of the power grid, we need to consider three aspects. (1) Improvement of the regulation ability of each component in the power system and the power grid itself. For example, when energy storage [21] and compensation [22], [23] devices are connected to the system, the resilience of the transmission capacity is strengthened [24]. (2) Improvement of planning and operation on different time scales, such as prediction [25], generation control [26], economic dispatch [27], ancillary services [28], and others. (3) Reasonable price and transaction mechanisms designed to meet the flexibility requirements of power system planning and operation, such as demand response [29], P2P trading [30], retail power markets [31], and others.

Simultaneously, power system dynamic optimal dispatching is a common multi-objective optimization problem with multiple decision variables, nonlinearity and strong coupling. The solution of power dispatch mathematical models involving large-scale grid-connected RES has become a subject of interest for scholars in China and abroad. In terms of model-solution, penalty factors [4], price penalty factors [10], hierarchical algorithms [6], column and constraint generation algorithms [10] are efficient and fast, but the process is complex and cannot be solved directly. If the model is non-differentiable and non-convex, the traditional methods above cannot be used to solve it, so feasibility and optimality are not guaranteed. Some algorithms for solving non-linear, non-convex, strongly coupled and complex constrained models are widely used, like hybrid biogeography-based optimization with brain storm optimization [32], shuffle frog leaping algorithm and particle swarm optimization [33], efficient fitness-based differential evolution [34], and the squirrel search algorithm [35]. However, with the development of large-scale RES integration and multi-energy coupling systems, the algorithm may terminate prematurely due to the lack of global optimization ability in the face of different complex optimization problems of modern power dispatching.

Based on the above analysis, we built a optimization model of day ahead dynamic game for CRIGs, which considers the generation economy and robustness of transmission sufficiency for each region. The two regions use the tie-line to interconnection, and choose their own strategies according to the possible strategies of the other side, to maximize their own interests under the strategy of the other side, so as to achieve Nash equilibrium. In the model, we consider the interconnection of tie-line areas and flexible loads. The uncertain source-load sets are constructed using robust optimization theory, the boundary of uncertain sets can be adjusted flexibly by introducing the uncertain spatial constraint parameters. Furthermore, according to the characteristics of the optimal scheduling model, we propose a hybrid evolutionary filter optimization (HEFO) to solve the above mixed-integer non-convex nonlinear programming problem. We use modified IEEE 39-bus systems and the power grid in the Hami region of Xinjiang as the case studies to analyze the model, verified the effectiveness and practicability of the model and algorithm. Accordingly, the main contributions of this paper are summarized as follow:

• We proposed a day-ahead optimization model for CRIGs, which considers the generation economy and robustness of transmission sufficiency for each region. Under the background of UHV transmission technology as the physical method of regional power interconnection, and centralized distribution of renewable energy power generation in China, the CRIGs can effectively alleviate imbalances between the power supply and demand across regions that result from large-scale and long-distance transmission.

• The a day-ahead optimization model considers the spatial clustering effect of RES and loads, uses robust optimization theory to construct uncertainty sets, and introduces uncertain spatial constraint parameters to overcome the shortcomings of traditional robust optimization while reasonably reducing the rotating reserve capacity and the blindness of dispatching cost. In actual operation, compared with traditional robust scheduling, the generation cost can be reduced by 21.9% under the premise of acceptable safe operation.

• According to the characteristics of the optimal scheduling model, we propose a hybrid evolutionary filter optimization (HEFO) to solve the above mixed-integer non-convex nonlinear programming problem.

We selected two interconnected modified IEEE 39-bus systems as the cross-area dispatching model, analyzed the dynamic dependence of uncertain variables on system economy and robustness, and explore most economical and reliable scheduling scheme under different decisions' demands by adjusting the parameters that restrict the aggregation of uncertainties, such as prediction accuracy and confidence probability etc. And the validity and feasibility of the proposed model and algorithm are verified on the power grid in the Hami region of Xinjiang.

II. CONSTRUCTION OF UNCERTAINTY SET

Taking wind power as an example, the uncertain output of each period for wind turbines can be described as follows:

$$\begin{cases} P_{\mathrm{W}i,t} = P^{\mathrm{S}}_{\mathrm{W}_{i,t}} + \Delta P_{\mathrm{W}i,t} \\ \Delta P^{l}_{\mathrm{W}_{i,t}} \le \Delta P_{\mathrm{W}i,t} \le \Delta P^{\mathrm{u}}_{\mathrm{W}_{i,t}}, \end{cases} \quad \forall_i, t \tag{1}$$

where $P_{\mathrm{W}i,t}$, $P^{\mathrm{S}}_{\mathrm{W}i,t}$, $\Delta P_{\mathrm{W}i,t}$ are the actual / predicted outputs and the output deviation of the i-th wind farm at time t. $\Delta P^{\mathrm{l}}_{\mathrm{W}i,t}$, $\Delta P^{\mathrm{u}}_{\mathrm{W}i,t}$ are the upper / lower limits of deviation.

Using robust theory to construct sets with additive uncertainties [7], we have:

$$\begin{aligned} p = \Big\{ & P_{\mathrm{W}i,\mathrm{t}} = P^{\mathrm{S}}_{\mathrm{W}_{i,t}} + \gamma_{\mathrm{W}i,\mathrm{t}} \cdot \Delta P^{\mathrm{u}}_{\mathrm{W}_{i,t}}, \forall i, t; \\ & \left\| \gamma_{\mathrm{W}i,\mathrm{t}} \right\|_\infty \le 1, \left\| \gamma_{\mathrm{W}_{i,t}} \right\|_1 \le \Gamma_{\mathrm{W}_t} \Big\} \\ \left\| \gamma_{\mathrm{W}i,\mathrm{t}} \right\|_\infty = & \max_{1 \le i \le N_{\mathrm{W}}} \left| \gamma_{\mathrm{W}_{i,t}} \right|, \left\| \gamma_{\mathrm{W}i,\mathrm{t}} \right\|_1 = \sum\nolimits_{i=1}^{N_{\mathrm{W}}} \left| \gamma_{\mathrm{W}_{i,t}} \right| \end{aligned} \tag{2}$$

where $||\gamma_{\mathrm{W}i,t}||_\infty$ denotes the infinite norm; $||\gamma_{\mathrm{W}i,t}||_1 \le \Gamma_{\mathrm{W}t}$ is a 1-norm constraint of perturbation, which corresponds to the spatial cluster effect of wind power output, thus the uncertain spatial constraint parameter $\tilde{a}_{\mathrm{W}t}$ is proposed; $\gamma_{\mathrm{W}i,t}$ is the deviation coefficient of the i-th wind farm at t. Suppose $\delta_{\mathrm{W}i,\mathrm{t}} = |\gamma_{\mathrm{W}i,t}|$. If $\Delta P_{\mathrm{W}i,t}$ is an independent and identically distributed random variable, then so is $\delta_{\mathrm{W}i,t}$, with an expectation of μ_{W} and variance of σ^2_{W}. According to the Lindeberg-Lévy central limit theorem, the standard variable $Y_{p\mathrm{W}}$ of sum $\sum_{i=1}^{N_{\mathrm{W}}} \delta_{\mathrm{W}i,\mathrm{t}}$ for $\delta_{\mathrm{W}i,t}$ obeys the standard normal distribution, and the cumulative distribution function $F_{p\mathrm{W}}(x)$ satisfies Eq. (3) for any probability distribution.

$$\begin{aligned} \lim_{N_W \to \infty} F_{pW}(x) &= \lim_{N_w \to \infty} P \left\{ \frac{\sum_{i=1}^{N_w} \delta_{wj} - N_w \mu_w}{\sqrt{N_W \sigma_W}} \le x \right\} \\ &= \int_{-\infty}^{x} \frac{1}{\sqrt{2\pi}} e^{\frac{\xi^2}{2}} d\xi = \Phi(x) = \alpha_w, \quad \forall t \end{aligned} \tag{3}$$

where α_{W} is the confidence probability. μ_{W}, and σ_{W} can be obtained by predictive and statistical data. It is assumed that $\Delta P_{\mathrm{W}i,t}$ follow a normal distribution [34], with an expectation of 0, and a variance of σ^*_{W}. Thus, $\Gamma_{\mathrm{W}t}$ can be deduced as follows:

$$\begin{aligned} \Gamma_{\mathrm{W},} = & N_{\mathrm{W}} \cdot \sqrt{\frac{2\sigma^{*2}_{\mathrm{W}}}{\pi}} \\ & + \Phi^{-1}(\alpha_{\mathrm{w}}) \sqrt{N_{\mathrm{W}} \cdot \left(\sigma^{*2}_{\mathrm{W}} - \frac{2\sigma^{*2}_{\mathrm{W}}}{\pi} \right)}, \quad \forall t \end{aligned} \tag{4}$$

Different from traditional robust optimization, the boundary for the set of uncertainties in Eq. (2) can be flexibly adjusted using $\Gamma_{\mathrm{W}t}$ according to the different α_{W} required by decision makers. For practical applications, the selection of the confidence probability and the influence of α_{W} on system dispatching are analyzed and explained in detail in Section III, Part C and Section V. Similarly, $\Gamma^{\mathrm{A}}_{\mathrm{L}t}$ and $\Gamma^{\mathrm{B}}_{\mathrm{L}t}$ of conventional loads in A / B regions can be derived using the uncertain sets $P^{\mathrm{A}}_{\mathrm{L}i,t}$ and $P^{\mathrm{B}}_{\mathrm{L}i,t}$.

III. ROBUST OPTIMAL DISPATCHING MODEL

A. CROSS-DISTRICT DISPATCHING MODE

Let us consider the interconnection of two areas A and area B through tie-lines, where A is the dispatching end with large-scale wind power resources, thermal units and conventional loads, while B is the receiving end, with relatively concentrated loads (thermal units, conventional loads, multiple adjustable loads), but no RES. Depending on their power consumption characteristics, loads can be divided into four categories:

(1) Conventional loads (CLs), which exhibit high randomness and are not scheduled;

(2) Transferable loads (TLs), for which the transfer compensation price coefficient is low;

(3) Peak catering loads (LSIs), where the load shedding rate is low (15%), while the compensation price index is high;

(4) Peak avoiding loads (LSII), where the load shedding rate is high (30%), but the compensation price index is low.

The sending-end transfers surplus power through the tie-line under the constraints of power consumption and tie-line planning. The receiving end consumes power through

coordinated dispatch of thermal units and adjustable loads to realize efficient power distribution among the regions and promote the consumption of new energy produced. During the optimization, information is updated and transmitted to each erea. Both A and B regions choose their own strategies according to the possible strategies of the other to ensure that their own interests are maximized under the other's strategies, So as to realize the dynamic game optimization among different regions.

B. MODEL SPECIFICATION

We take into consideration the consumption of thermal units, the cost of flexible load dispatching and the rotating reserves:

$$\min f = \sum_{t=1}^{T}\left(\sum_{i=1}^{N_{\mathrm{GA}}} C_{i,t}^{\mathrm{A}}\left(P_{\mathrm{G}i,t}^{\mathrm{A}}\right)+\sum_{i=1}^{N_{\mathrm{GB}}} C_{i,t}^{\mathrm{B}}\left(P_{\mathrm{G}it}^{\mathrm{B}}\right)\right) + f_{\mathrm{esu}} + f_{\mathrm{el}} + f_{\mathrm{ek}} \quad (5)$$

where T is the total dispatching cycle. N_{GA}, N_{GB} are the number of thermal units in A and B, respectively, and $P_{\mathrm{G}i,t}^{\mathrm{A}}$, $P_{\mathrm{G}i,t}^{\mathrm{B}}$ are the outputs of the i-th unit at t in A and B. $C_{i,t}^{\mathrm{A}}(P_{\mathrm{G}i,t}^{\mathrm{A}})$, and $C_{i,t}^{\mathrm{B}}(P_{\mathrm{G}i,t}^{\mathrm{B}})$ (h / \$) denote the total thermal generation cost; considering the valve point effect, that is a pulse which will be superimposed on the energy consumption curve [36]. The valve point effect makes the energy consumption curve of generating units no longer smooth quadratic convex function, but non convex and non smooth [37], [38]. f_{esu} is the start-up / shutdown cost of the thermal units, f_{el}, f_{ek} are the cost of flexible loads dispatching and rotating reserves (taking A as an example in (6)-(9)):

$$\sum_{i=1}^{N_{\mathrm{GA}}} C_{i,t}^{\mathrm{A}}\left(P_{\mathrm{G}i,t}^{\mathrm{A}}\right) = y_{i,t}^{\mathrm{A}}\left\{a_i^{\mathrm{A}} + b_i^{\mathrm{A}} P_{\mathrm{G}i,t}^{\mathrm{A}} + c_i^{\mathrm{A}}\left(P_{\mathrm{G}i,t}^{\mathrm{A}}\right)^2 + \left|d_i^{\mathrm{A}}\sin\left[e_i^{\mathrm{A}}\left(P_{\mathrm{G}i,\min}^{\mathrm{A}} - P_{\mathrm{G}i,t}^{\mathrm{A}}\right)\right]\right|\right\} \quad (6)$$

$$f_{\mathrm{esu}} = \sum_{t=1}^{T}\left\{\sum_{i=1}^{N_{\mathrm{GA}}}\left(S_{\mathrm{on},i} FN_{i,t}^{\mathrm{A}} + S_{\mathrm{off},i} NF_{i,t}^{\mathrm{A}}\right) + \sum_{i=1}^{N_{\mathrm{GB}}}\left(S_{\mathrm{on},i} FN_{i,t}^{\mathrm{B}} + S_{\mathrm{off},i} NF_{i,t}^{\mathrm{B}}\right)\right\} \quad (7)$$

where, a_i, b_i, $c_i d_i$, and e_i are the fuel cost and threshold effect coefficients, $S_{\mathrm{on},I}$, $S_{\mathrm{off},i}$ are the unit start-up cost coefficients, $y_{i,t}$, $FN_{i,t}$, $NF_{i,t}$ are the operational / start-up / shutdown state of thermal units. If a thermal unit is running, $y_{\mathrm{i,t}}$ is 1, otherwise it is 0. If the state of a thermal unit changes from shutdown to start-up, $FN_{i,t}$ is 1, otherwise it is 0. If it changes from start-up to shutdown, $NF_{i,t}$ is 1. $P_{\mathrm{LT}i,t} > 0$ represents load removal, while a negative value indicates load attachment. ξ_{LSI}, ξ_{LSII}, ξ_{LT} are the dispatching cost coefficients of LSI / LSII / TL while $P_{\mathrm{LSI}t}$, $P_{\mathrm{LSII}t}$, $P_{\mathrm{LT}t}$ are the corresponding scheduled powers. $k_{\mathrm{W}i}$, $k_{\mathrm{L}i}$ are penalty coefficients of spinning reserve cost for wind turbine / load.

$$f_{\mathrm{el}} = \sum_{t=1}^{T}\left(\xi_{\mathrm{LST}}\cdot P_{\mathrm{LS}_t} + \xi_{\mathrm{SSII}}\cdot P_{\mathrm{LSII}_t} + \xi_{\mathrm{LT}}\cdot \mid P_{\mathrm{LT}_1}\right) \quad (8)$$

$$f_{\mathrm{ek}} = \sum_{t=1}^{T}\left\{\sum_{i=1}^{N_{\mathrm{W}}} k_{\mathrm{W}i}\gamma_{\mathrm{W}_{i,t}}\Delta P_{\mathrm{W}_{i,t}}^{\mathrm{u}} + \sum\nolimits_{i=1}^{N_{\mathrm{L}}^{\mathrm{A}}} k_{\mathrm{L}i}^{\mathrm{A}} f_{k\mathrm{A}} + \sum\nolimits_{i=1}^{N_{\mathrm{L}}^{\mathrm{B}}} k_{\mathrm{L}i}^{\mathrm{B}} f_{\mathrm{kB}}\right\}$$

$$\text{where, } f_{\mathrm{kA}} = \begin{cases} \Delta P_{\mathrm{L}_{i,t}}^{\mathrm{A}} P_{L_{j,t}}^{\mathrm{A\text{-}h}}, & \Delta P_{\mathrm{L}_{i,t}}^{\mathrm{A}} > 0 \\ 0, & \Delta P_{\mathrm{L}_{i,t}}^{\mathrm{A}} \le 0 \end{cases} \quad (9)$$

In the above objective optimization, the following constraints must be met:

(1)Power balance constraints: Sending end:

$$\sum_{i=1}^{N_{\mathrm{GA}}} P_{\mathrm{G}_{i,t}}^{\mathrm{A}}\cdot y_{i,t}^{\mathrm{A}} + \sum_{i=1}^{N_{\mathrm{W}}} P_{\mathrm{W}_{i,t}} = \sum\nolimits_{i=1}^{N_{\mathrm{L}}^{\mathrm{A}}} P_{\mathrm{L}_{i,t}}^{\mathrm{A}} + P_t^{\mathrm{dc}}, \quad \forall t \quad (10)$$

Receiving end:

$$\sum_{i=1}^{N_{\mathrm{GB}}} P_{\mathrm{G}_{i,t}}^{\mathrm{B}}\cdot y_{i,t}^{\mathrm{B}} + P_t^{\mathrm{dc}} = \sum_{i=1}^{N_{\mathrm{L}}^{\mathrm{B}}} P_{\mathrm{L}_{i,t}}^{\mathrm{B}} - P_{\mathrm{LSI}_t} - P_{\mathrm{LSII}_t} - P_{\mathrm{LT}_t}, \ \forall t \quad (11)$$

where P_t^{dc}, is the scheduling power of the tie-line.

(2) Operational constraints of thermal units (taking area A as an example, B is the same):

$$y_{i,t}^{\mathrm{A}} P_{\mathrm{G}i,\min}^{\mathrm{A}} \le P_{\mathrm{G}_{i,t}}^{\mathrm{A}} \le y_{i,t}^{\mathrm{A}} P_{\mathrm{G}i,\mathrm{mos}}^{\mathrm{A}}, \quad \forall i,t \quad (12)$$

$$P_{\mathrm{G}_{i,t}}^{\mathrm{A}} - P_{\mathrm{G}_{i,(t-1)}}^{\mathrm{A}} \le y_{i,t}^{\mathrm{A}} R_{\mathrm{U}_i}^{\mathrm{A}} + \left(1 - y_{i,(t-1)}^{\mathrm{A}}\right) P_{\mathrm{G}i,\max}^{\mathrm{A}} + P_{\mathrm{G}i,\min}^{\mathrm{A}}\left(y_{i,t}^{\mathrm{A}} - y_{i,(t-1)}^{\mathrm{A}}\right), \quad \forall i,t \quad (13)$$

$$P_{\mathrm{G}_{i,(t-1)}}^{\mathrm{A}} - P_{\mathrm{G}_{i,t}}^{\mathrm{A}} \le y_{i,t}^{\mathrm{A}} R_{\mathrm{D}_i}^{\mathrm{A}} + \left(1 - y_{i,(t-1)}^{\mathrm{A}}\right) P_{\mathrm{G}i,\max}^{\mathrm{A}} + P_{\mathrm{G}i,\min}^{\mathrm{A}}\left(y_{i,(t-1)}^{\mathrm{A}} - y_{i,t}^{\mathrm{A}}\right), \quad \forall i,t \quad (14)$$

$$-y_{i,(t-1)}^{\mathrm{A}} + y_{i,t}^{\mathrm{A}} - y_{i,k}^{\mathrm{A}} \le 0, \quad \forall i,t; t \le k \le T_{\mathrm{on},i}^{\mathrm{A}} + t - 1 \quad (15)$$

$$y_{i,(t-1)}^{\mathrm{A}} - y_{i,t}^{\mathrm{A}} + y_{i,k}^{\mathrm{A}} \le 1, \quad \forall i,t; t \le k \le T_{\mathrm{off},i}^{\mathrm{A}} + t - 1 \quad (16)$$

$$-y_{i,(t-1)}^{\mathrm{A}} + y_{i,t}^{\mathrm{A}} - FN_{i,t}^{\mathrm{A}} \le 0, \quad \forall i,t \quad (17)$$

$$y_{i,(t-1)}^{\mathrm{A}} - y_{i,t}^{\mathrm{A}} - NF_{i,t}^{\mathrm{A}} \le 0, \quad \forall i,t \quad (18)$$

Eq. (12) denotes the unit output constraint, Eqs. (13)-(14) denote the climbing constraints, Eqs. (15)-(16) denote the minimum start-up time constraints, and Eqs. (17)-(18) represent the logical relationship between running and start-stop state variables. $T_{\mathrm{on},I}^{\mathrm{A}}$, $T_{\mathrm{off},i}^{\mathrm{A}}$ are the minimum start-up and shutdown times of the thermal units.

(3) Flexible load dispatching constraints

$$0 \le P_{\mathrm{LSI}_t} \le P_{\mathrm{R}_t}^{\mathrm{F}}\cdot\lambda_{\mathrm{LS}I}\cdot 15\%, \forall t \quad (19)$$

$$0 \le P_{\mathrm{LS}II_t} \le P_{\mathrm{R}_t}^{\mathrm{F}}\cdot\lambda_{\mathrm{LS}II}\cdot 30\%, \forall t \quad (20)$$

$$-P_{\mathrm{R}_t}^{\mathrm{F}}\cdot\lambda_{\mathrm{LT}} \le P_{\mathrm{LT}_t} \le P_{\mathrm{R}_t}^{\mathrm{F}}\cdot\lambda_{\mathrm{LT}}, \forall t \quad (21)$$

$$\sum_{t=1}^{T} P_{\mathrm{LS}II_t} = 0 \quad (22)$$

where $P_{\mathrm{R}t}^{\mathrm{F}}$ are the total loads at t.

(4) Tie-line constraints

$$P^{\mathrm{dc}}_{\mathrm{down}} \le P^{\mathrm{dc}}_{t} - P^{\mathrm{dc}}_{t-1} \le P^{\mathrm{dc}}_{\mathrm{up}}, \quad \forall t \tag{23}$$

$$P^{\mathrm{dc}}_{1} \le P^{\mathrm{dc}}_{t} \le P^{\mathrm{dc}}_{\mathrm{u}}, \quad \forall t \tag{24}$$

$$P^{\mathrm{dc}}_{t} = P^{\mathrm{dc}}_{t+k}, P^{\mathrm{dc}}_{t-1} \ne P^{\mathrm{dc}}_{t}, \quad \forall t; 1 \le i \le t_{\mathrm{n}} \tag{25}$$

where $P^{\mathrm{dc}}_{\mathrm{down}}$, $P^{\mathrm{dc}}_{\mathrm{up}}$ are the upper and lower climbing limits for tie-line power. t_{n} is the minimum maintenance time. P^{dc}_{1}, $P^{\mathrm{dc}}_{\mathrm{u}}$ are the permissible upper and lower power limits for the tie-line.

(5) The regional rotation reserve constraints are shown in Eqs. (26)-(27), where L is the rotation reserve rate (%).

(6) Security constraints are shown in Eqs. (28)-(29), where $P_{l,\max}$ is the transmission power limit of line l., while $Tr_{\mathrm{G}i}$, Tr_{dc}, $Tr_{\mathrm{W}i}$, $Tr_{\mathrm{L}i}$, $Tr_{\mathrm{R}i}$ the transfer distribution factors of thermal units / wind generators / conventional loads / flexible loads / tie-lines, respectively.

Sending end:

$$\sum_{i=1}^{N_{\mathrm{GA}}} P^{\mathrm{A}}_{\mathrm{G}_{i,\max}} y^{\mathrm{A}}_{\mathrm{i,t}} + \sum_{i=1}^{N_{\mathrm{W}}} P_{\mathrm{W}_{i,t}} \ge \left(\sum\nolimits_{i=1}^{N^{\mathrm{A}}_{\mathrm{L}}} P^{\mathrm{A}}_{\mathrm{L}_{i,t}} + P^{\mathrm{dc}}_{t}\right)(1+L\%), \quad \forall t \tag{26}$$

Receiving end:

$$\sum_{i=1}^{N_{\mathrm{GB}}} P^{\mathrm{B}}_{\mathrm{G}_{i,\max}} y^{\mathrm{B}}_{i,t} + P^{\mathrm{dc}}_{t} \ge \left(\sum\nolimits_{i=1}^{N^{\mathrm{B}}_{\mathrm{L}}} P^{\mathrm{B}}_{\mathrm{L}_{i,t}} - P_{\mathrm{LS\,I}_t} - P_{\mathrm{LSII}_t} - P_{\mathrm{LT}_t}\right)(1+L\%), \ \forall t \tag{27}$$

Sending end:

$$\left\{\sum_{i=1}^{N_{\mathrm{GA}}} Tr^{\mathrm{A}}_{\mathrm{G}_i} P^{\mathrm{A}}_{\mathrm{G}_{i,t}} y^{\mathrm{A}}_{i,t} - Tr^{\mathrm{A}}_{\mathrm{dc}} P^{\mathrm{dc}}_{t} + \sum_{i=1}^{N_{\mathrm{W}}} Tr^{\mathrm{A}}_{\mathrm{W}_i} P_{\mathrm{W}_{i,t}} - \sum_{i=1}^{N^{\mathrm{A}}_{\mathrm{L}}} Tr^{\mathrm{A}}_{\mathrm{L}_i} P^{\mathrm{A}}_{\mathrm{L}_{i,t}}\right\} \le P^{\mathrm{A}}_{l,\max}, \quad \forall t \tag{28}$$

Receiving end:

$$\left\{\sum_{i=1}^{N_{\mathrm{GB}}} Tr^{\mathrm{B}}_{\mathrm{G}_i} P^{\mathrm{B}}_{\mathrm{G}_{i,t}} y^{\mathrm{B}}_{i,t} - \sum_{i=1}^{N^{\mathrm{B}}_{\mathrm{L}}} Tr^{\mathrm{B}}_{\mathrm{L}_i} P^{\mathrm{B}}_{\mathrm{L}_{i,t}} + Tr^{\mathrm{B}}_{\mathrm{dc}} P^{\mathrm{dc}}_{t} - Tr^{\mathrm{B}}_{\mathrm{R}}\left(\sum_{i=1}^{N^{\mathrm{B}}_{\mathrm{L}}} P^{\mathrm{B}}_{\mathrm{L}_{i,t}} - P_{\mathrm{LSI}_t} - P_{\mathrm{LS}II_t} - P_{\mathrm{LT}_t}\right)\right\} \le P^{\mathrm{B}}_{l,\max}, \ \forall t \tag{29}$$

C. DISPOSING AND DECISION MAKING FOR UNCERTAINTY

Robust optimal dispatching requires that the system can still meet the operation requirements in the worst case of uncertain variables, and obtain the most economical operation dispatch of the system. This part is to analyze the safe operation of the system in extreme cases.

The uncertainty descriptions of A's and B's regional loads are similar to Eq. (1). N^A_L and N^B_L are the total numbers of loads in A and B. $P^{\mathrm{A}}_{\mathrm{L}i,t}$, $P^{\mathrm{A-S}}_{\mathrm{L}i,t}$, $\Delta P^{\mathrm{A}}_{\mathrm{L}i,t}$, $\Delta P^{\mathrm{A-u}}_{\mathrm{L}i,t}$, $\Delta P^{\mathrm{A-l}}_{\mathrm{L}i,t}$, $\gamma^{\mathrm{A}}_{\mathrm{L}i,t}$, are the actual / planned / deviation and upper / lower limits of the deviation, and $\Gamma^{\mathrm{A}}_{\mathrm{L},t}$ is the spatial constraints of the load in area A. Area B has the same variables as above, which are distinguished using superscript B. The uncertainty description and uncertainty set formulation for loads in A and B are the same as those for the wind power output.

The uncertain variables of the model are treated as follows: the uncertain description of load in A and Eq. (10) are introduced into Eq. (26) and the variables $\sum_{i=1}^{N^{\mathrm{A}}_{\mathrm{L}}} P^{\mathrm{A}}_{\mathrm{L}_{i,t}}$ and $\sum_{i=1}^{N_{\mathrm{W}}} P_{\mathrm{W}_{i,t}}$ are eliminated to obtain Eqs. (30) and (31). By formulating the Lagrange function and using linear duality theory, we obtain

$$\begin{aligned}
&\max\left(\sum_{i=1}^{N_{\mathrm{W}}} \Delta P_{\mathrm{W}i,t}\right) \\
&\quad = -\sum_{i=1}^{N_{\mathrm{W}}} \gamma_{\mathrm{W}_{i,t}} \Delta P^{\mathrm{u}}_{\mathrm{W}_{i,t}}, \max\left(\sum_{i=1}^{N^{\mathrm{A}}_{\mathrm{L}}} P^{\mathrm{A}}_{\mathrm{L}_{i,t}}\right) \\
&\quad = \sum_{i=1}^{N^{\mathrm{A}}_{\mathrm{L}}} \left(P^{\mathrm{A\text{-}S}}_{\mathrm{L}_{i,t}} + \gamma^{\mathrm{A}}_{\mathrm{L}_{i,t}} \Delta P^{\mathrm{A\text{-}u}}_{\mathrm{L}_{i,t}}\right).
\end{aligned}$$

$$\max\left(\sum_{i=1}^{N_{\mathrm{W}}} \Delta P_{\mathrm{W}i,t}\right) \le \frac{\sum_{i=1}^{N_{\mathrm{GA}}} P^{\mathrm{A}}_{\mathrm{G}_{i,\max}} y^{\mathrm{A}}_{i,t} - \sum_{i=1}^{N_{\mathrm{GA}}} P^{\mathrm{A}}_{\mathrm{G}_{i,t}} y^{\mathrm{A}}_{i,t}(1+L\%)}{L\%} - \sum_{i=1}^{N_{\mathrm{GA}}} P^{\mathrm{S}}_{\mathrm{W}_{i,t}} \tag{30}$$

$$\max\left(\sum_{i=1}^{N^{\mathrm{A}}_{\mathrm{L}}} P^{\mathrm{A}}_{\mathrm{L}_{i,t}}\right) \le \frac{\sum_{i=1}^{N_{\mathrm{GA}}} P^{\mathrm{A}}_{\mathrm{G}_{i,\max}} y^{\mathrm{A}}_{i,t} - \sum_{i=1}^{N_{\mathrm{GA}}} P^{\mathrm{A}}_{\mathrm{G}i,t} y^{\mathrm{A}}_{i,t}}{L\%} - P^{\mathrm{dc}}_{t} \tag{31}$$

The uncertainty description of loads in area B and Eq. (11) are introduced into Eq. (27) to obtain Eq. (32), and the corresponding expression: $\max\left(\sum_{i=1}^{N^{\mathrm{B}}_{\mathrm{L}}} P^{\mathrm{B}}_{\mathrm{L}_{i,t}}\right) = \sum_{i=1}^{N^{\mathrm{B}}_{\mathrm{L}}} \left(P^{\mathrm{B\text{-}S}}_{\mathrm{L}_{i,t}} + \gamma^{\mathrm{B}}_{\mathrm{L}_{i,t}} \Delta P^{\mathrm{B\text{-}u}}_{\mathrm{L}_{i,t}}\right)$. Based on the above analysis we can obtain the lower and upper limits of the uncertain sets of wind generator output and CLs reach the lower and upper limits in the extreme case.

$$\max\left(\sum_{i=1}^{N^{\mathrm{B}}_{\mathrm{L}}} P^{\mathrm{B}}_{\mathrm{L}_{i,t}}\right) \le \frac{\sum_{i=1}^{N_{\mathrm{GR}}} P^{\mathrm{B}}_{\mathrm{G}_{i.\,\max}} y^{\mathrm{B}}_{i,t} - \sum_{i=1}^{N_{\mathrm{GR}}} P^{\mathrm{B}}_{\mathrm{G}_{i,t}} y_{i,t}}{L\%} - \left(\sum_{i=1}^{N^{\mathrm{B}}_{\mathrm{L}}} P^{\mathrm{B}}_{\mathrm{L}_{i,t}} - P_{\mathrm{LSI}_t} - P_{\mathrm{LSII}_t} - P_{\mathrm{LT}_t}\right) \tag{32}$$

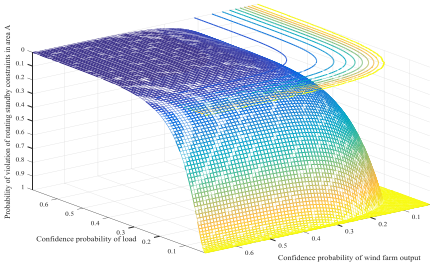

FIGURE 1. Probability relation of constraint violation in area A.

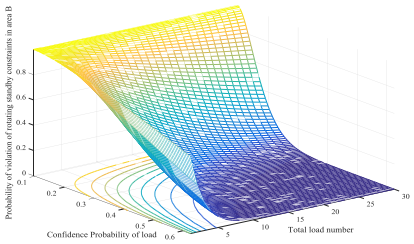

FIGURE 2. Probability relation of constraint violation in area B.

We consider the most extreme situation at t, where the deviation coefficient of only one wind farm output and load are less than 1. If the wind farm is j, the total wind power output and the total CLs in the case of area A are as shown in Eq. (33) and (34).

$$\sum_{i=1}^{N_{\mathrm{W}}} P_{\mathrm{W}i,t} = \sum_{i=1}^{N_{\mathrm{W}}-1} \left(P^{\mathrm{S}}_{\mathrm{W}i,t} - \Delta P^{\mathrm{u}}_{\mathrm{W}i,t}\right) + P^{\mathrm{S}}_{Wj,t} - \left(\Gamma_{\mathrm{W},t} - \left[\Gamma_{\mathrm{W},t}\right]\right) \Delta P^{\mathrm{u}}_{\mathrm{W}j,t} \tag{33}$$

$$\sum_{i=1}^{N^{\mathrm{A}}_{\mathrm{L}}} P^{\mathrm{A}}_{\mathrm{L}i,t} = \sum_{i=1}^{N^{\mathrm{A}}_{\mathrm{L}}-1} \left(P^{\mathrm{A\text{-}S}}_{\mathrm{L}i,t} + \Delta P^{\mathrm{A\text{-}u}}_{\mathrm{L}i,t}\right) + P^{\mathrm{A\text{-}S}}_{\mathrm{L}j,t} - \left(\Gamma^{\mathrm{A}}_{\mathrm{L},t} - \left[\Gamma^{\mathrm{A}}_{\mathrm{L},t}\right]\right) \Delta P^{\mathrm{A\text{-}u}}_{\mathrm{L}j,t} \tag{34}$$

where $[\cdot]$ is the ceiling symbol. The probability that in area A the system cannot satisfy the spinning reserve constraint is shown in Eq. (35).

$$\begin{aligned} P &\left\{ \sum_{i=1}^{N_{\mathrm{GA}}} P^{\mathrm{A}}_{\mathrm{G}i,\max} y^{\mathrm{A}}_{i,t} + \sum\nolimits_{i=1}^{N_{\mathrm{W}}} P_{\mathrm{W}i,t} \right. \\ &\left. < \left(\sum\nolimits_{i=1}^{N^{\mathrm{A}}_{\mathrm{L}}} P^{\mathrm{A}}_{\mathrm{L}i,t} + P^{\mathrm{dc}}_{t} \right) (1 + L\%) \right\} \\ &\leq \exp\left(-\frac{\Gamma^2_{\mathrm{W},t}}{2N_W} \right) + \exp\left(-\frac{\left(\Gamma^{\mathrm{A}}_{\mathrm{L},t}\right)^2}{2N^{\mathrm{A}}_{\mathrm{L}}} \right) \\ &\quad + \exp\left(-\frac{\Gamma^2_{\mathrm{W},t}}{2N_{\mathrm{W}}} - \frac{\left(\Gamma^{\mathrm{A}}_{\mathrm{L},t}\right)^2}{2N^{\mathrm{A}}_{\mathrm{L}}} \right) \end{aligned} \tag{35}$$

By introducing Eq. (4) into Eq. (35), the relationship between the rotating reserve violation probability in area A and the confidence probability of both wind farm output and load uncertainty sets can be obtained as shown in Fig. 1 (assuming both wind plants and total loads are 30). Similarly, the probability of backup violation in area B is given in Eq. (36).

$$P \left\{ \sum_{i=1}^{N_{\mathrm{GB}}} P^{\mathrm{B}}_{G_{i,\max}} y^{\mathrm{B}}_{i,t} + P^{\mathrm{dc}}_{t} < \left(\sum\nolimits_{i=1}^{N^{\mathrm{B}}_{\mathrm{L}}} P^{\mathrm{B}}_{\mathrm{L}i,t} - P_{\mathrm{LSI}_t} - P_{\mathrm{LSII}_t} - P_{\mathrm{LT}_t} \right) (1 + L\%) \right\} \leq \exp\left(-\frac{\left(\Gamma^{\mathrm{B}}_{\mathrm{L},t}\right)^2}{2N^{\mathrm{B}}_{\mathrm{L}}} \right) \tag{36}$$

From Figs. 1 and 2, we see that the rotating reserve violation probability in area A decreases continuously with the increase in the confidence probability. As the number of loads decreases in area B, the violation probability increases correspondingly. Therefore, the system conservatism can be reduced by flexibly adjusting the confidence probability of uncertain sets. In this manner, the prediction accuracy can be improved, which is also an effective way to reduce the scheduling conservatism. (The above graphical analysis is based on the standard normal distribution of deviations, when the prediction accuracy is only 68.27%.)

Decision makers must weigh the probability of violating system security constraints and system economy according to the requirements and characteristics of the system. The economy of the system can be increased through an informed reduction of the confidence probability, or the robustness of the system can be improved by improving the prediction accuracy of uncertain variables and increasing the confidence probability. After fully balancing economy and conservatism, the obtained plan is both robust and optimally scheduled. It is worth noting that we quantify the robustness of the system and evaluate it through the probability of exceeding the system security constraints. Different from traditional robust optimization approaches, we do not optimize the system under the premise of 100% security and stability, because the results obtained in this case are too conservative at the expense of system economy. We maintain the probability of exceeding the system security constraints at a low level close to 0, or control the probability within a range that is acceptable by decision makers.

IV. COLLABORATIVE EVOLUTIONARY SOLUTION BASED ON FILTER TECHNOLOGY

The robust optimal dispatching model is an optimization problem for thermal unit operation, flexible loads and tie-line planning in an uncertain environment (The power of the tie-line is discretized to a multiple of 10 to ensure smooth running and prevent excessive burrs.). For the uncertain variables $(P^{\mathrm{A}}_{\mathrm{L}i,t}, P^{\mathrm{B}}_{\mathrm{L}i,t}, P_{\mathrm{W}i,t})$ in the system, we establish the uncertain set in the manner presented in section II. We explore the relationship between the probability of the system exceeding security constraints and the dispatching results under different confidence probabilities. Considering both economy and robustness combined with the actual situation and decision

demands, the most appropriate confidence probabilities are selected to optimize the following decision variables: the Boolean variables $y_{i,t}$, $FN_{i,t}$, $NF_{i,t}$, the discrete variable P_t^{dc}, and the continuous variables $P_{\mathrm{G}i,t}$, $P_{\mathrm{LSI}t}$, $P_{\mathrm{LSI}t}$, and $P_{\mathrm{LT}t}$. The general form is shown in (37).

$$\begin{cases} \min f(X, Y, Z) \\ s.t.g(X, Y, Z) \leq 0; \\ h(X, Y, Z) = 0; \\ X_{\min} \leq X \leq X_{\max}, Z_{\min} \leq Z \leq Z_{\max} \end{cases} \tag{37}$$

where, $\boldsymbol{X} = [x_1, x_2, \ldots, x_n]$, $\boldsymbol{Y} = [y_1, y_2, \ldots, y_n]$ and $\boldsymbol{Z} = [z_1, z_2, \ldots, z_n]$ represent continuous / Boolean / discrete variables, $f(\boldsymbol{X}, \boldsymbol{Y}, \boldsymbol{Z})$ represents the objective function, and $g(\boldsymbol{X}, \boldsymbol{Y}, \boldsymbol{Z})$, $h(\boldsymbol{X}, \boldsymbol{Y}, \boldsymbol{Z})$ represent the inequality / equality constraints. In order to solve the above mixed-integer non-convex nonlinear programming problem, a co-evolutionary algorithm based on filtering is proposed. The algorithm is based on the evolutionary principle of species, so we adopt a multi-population coordination mechanism, which includes an improved moth-flame optimization (IMFO) for continuous variables, a differential evolution (DE) algorithm for discrete variables and a genetic algorithm (GA) for Boolean variables.

A. FILTER TECHNOLOGY

We form a number pair (F, G) consisting of an objective function and a constraint violation degree to represent the filter, where, $\mathrm{F} = f(\boldsymbol{X}, \boldsymbol{Y}, \boldsymbol{Z})$, while G is defined in (38). Like the minimum value problem, the filtering approach has the following definitions [39].

$$\mathrm{G} = \max(0, g(\boldsymbol{X}, \boldsymbol{Y}, \boldsymbol{Z})) + \mathrm{abs}(h(\boldsymbol{X}, \boldsymbol{Y}, \boldsymbol{Z})) \tag{38}$$

Definition 1: If $\mathrm{F}(x_i) \leq \mathrm{F}(x_j)$, and $\mathrm{G}(x_i) \leq \mathrm{G}(x_j)$, it is said that filter $(\mathrm{F}(x_i)), \mathrm{G}(x_i))$ dominates filter $(\mathrm{F}(x_j)), \mathrm{G}(x_j))$.

Definition 2: Filters in filter set do not dominate each other.

B. ALGORITHMIC FLOW

In the proposed hybrid evolutionary filter optimization (HEFO), the positions of individuals in space correspond to decision variables in the optimal scheduling problem. Eqs. (10)-(11) correspond to $h(\boldsymbol{X}, \boldsymbol{Y}, \boldsymbol{Z})$, while Eqs. (26)-(29) correspond to $g(\boldsymbol{X}, \boldsymbol{Y}, \boldsymbol{Z})$. For other inequality constraints, which can be treated as boundary limits, we leverage the advantages of metaheuristic algorithms (IMFO, GA and DE are heuristic algorithms). The detailed steps of solving the optimal scheduling model using HEFO are shown in Fig. 3.

The continuous variables are optimized using the IMFO. Moth-flame optimization (MFO) was proposed by Mirjalili in 2015. It originated from the lateral positioning navigation mode of moths during night flight [40]. The location of moths in the search space is updated using a logarithmic spiral operator. Exploration and exploitation are balanced effectively in (39), which describes the helical flight path of moth. The discrete variables are optimized using the GA, which generates a new population through a series of operations including selection, crossover and mutation of the current

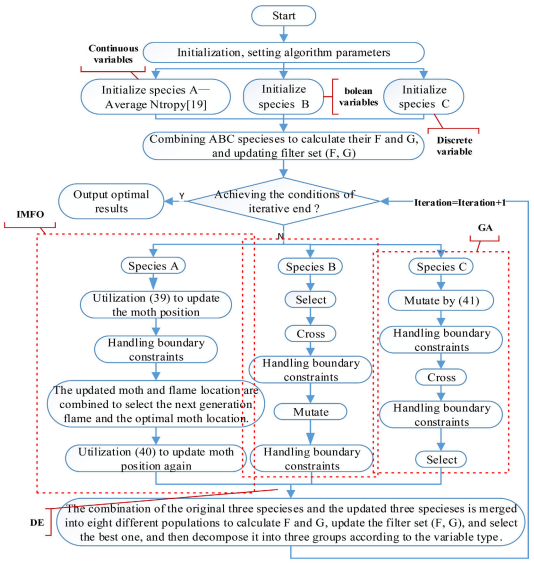

FIGURE 3. Algorithm flow chart.

population. The GA is efficient and has good adaptability. The Boolean variables are optimized using the DE, which is a stochastic heuristic search algorithm. The DE has strong robustness and global search ability.

$$\begin{aligned} M_i^{N+1} &= D_i \cdot e^{bt} \cdot \cos(2\pi t) + F_j \\ D_i &= |F_j - M_i| \end{aligned} \tag{39}$$

where, superior N denotes the current number of iterations, M is the moth position, F is the flame position, which is the optimal position for moths currently, b is a logarithmic helix shape constant, t is a random number between $[-1, 1]$ denoting the distance of the moth's next generation from its corresponding flame ($t = -1$ is the nearest and $t = 1$ is the farthest).

$$\begin{aligned} M_i^{N+1} &= M_i^N + \partial \oplus L(\lambda) \oplus (M_i^N - best), \quad i = 1 \ldots \dim \\ L(\lambda) &= \left| \frac{\Gamma(1+\lambda)^* \sin(\frac{\pi\lambda}{2})}{\Gamma(\frac{1+\lambda}{2})^* \lambda^* 2^{(\frac{\lambda-1}{2})}} \right|^{\frac{1}{\lambda}} \end{aligned} \tag{40}$$

In order to increase the diversity of the population and avoid the premature termination of the algorithm, Lévy flight strategy is added to the MFO. Eq. (40) illustrates the process of Lévy flight strategy, where $\oplus$ denotes point-to-point multiplication, ∂ is the step size control factor, *best* is the best location of the moth, $L(\lambda)$ is the Lévy random search subject to the Lévy distribution, and λ is a constant between [1, 3].

The solution of the DE is updated as follows:

$$V_i^G = X_{r1}^G \otimes \left(X_{r2}^G \otimes X_{r3}^G \right) \tag{41}$$

where, $r1$, $r2$, $r3 \in [1, \mathrm{NP}]$ are the non-repetitive random variables, NP is the population size, X corresponds to the decision variables of species B, and $\otimes$ is the XOR logical operator.

TABLE 1. Operating parameters of conventional unit and tie-line.

NO.	Upper	Lower	Minimum stop-start time(h)	Climbing(MW/h)	stop-start cost(MW/ $)
1	470	150	8	141	20000
2	470	135	8	141	20000
3	340	73	5	102	15000
4	300	60	5	90	15000
5	243	73	6	72.9	10000
6	180	57	3	54	6750
7	130	20	3	39	6750
8	120	47	1	36	6750
9	80	20	1	24	5000
10	55	10	1	16.5	5000
Tie-line	400	150	-	120	-

V. CASE STUDY

A. CASE 1: MODIFIED IEEE-39 BUS SYSTEM

In this case, we select two interconnected IEEE 39-bus systems as the cross-area dispatching model. A single area system consists of 10 conventional units and 46 transmission lines. The line reactance and allowable maximum power flow are 0.3p.u and 200 MW, respectively. The regional converter stations are located at the 7th and 27th nodes of the sending and receiving ends, respectively. The wind farm and the controllable loads are connected to nodes 29 and 25 at the receiving end. The average predicted outputs of the wind farm and the conventional loads at both ends are in Fig. 4. The system operation parameters are provided in Tables 1-4.

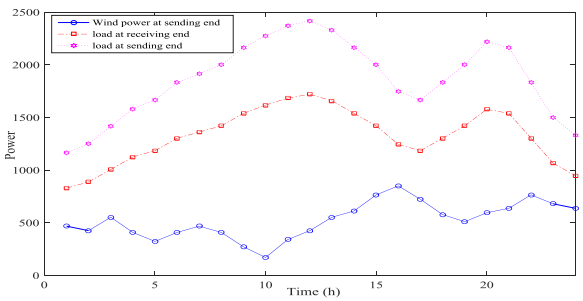

FIGURE 4. Mean value of load and wind output prediction.

TABLE 2. Flexible load settings.

	CL	TL	LSI	LSII
percentage	30%	20%	20%	30%
Cost of invoking (KWh/$)	-	0.25	0.5	0.3

TABLE 3. Penalty coefficients.

Coefficient of rotary standby penalty(MW/ $)		
Wind plants output	Loads in A	Loads in B
600	600	600

1) INFLUENCE OF CONFIDENCE PROBABILITY

First, we study the effect of different confidence probabilities on scheduling results. We set the prediction accuracy as

TABLE 4. Algorithmic settings.

Maximum iterations	1000	Helical constant b	1
Population size *pop*	150	*Logistic*.max	50
Flame.max	150	Mutation rate of DE	0.5
Mutation rate of GA	0.1	Crossing rate of DE	0.9
Crossing rate of GA	0.8		

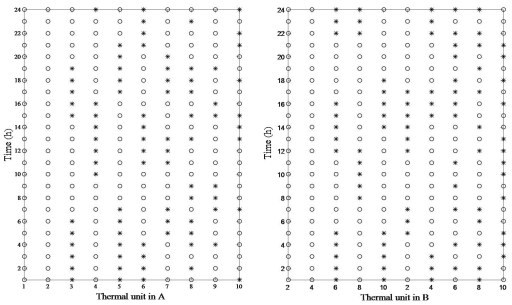

FIGURE 5. Operational status of units ($\alpha = 0.6$, 68.27%).

68.27%, the number of wind farms to 30, and the number of loads in A / B are 20 / 30, respectively. Different confidence probabilities were selected and the results are shown in Table 5.

As the confidence probability decreases, the interval of uncertain sets shrinks, the cost of rotating reserve and flexible dispatching decreases, and the dispatching economy increases. It should be noted that the total cost does not have a linear relationship with the confidence probability. When $\alpha < 20\%$, there is little change in the total cost, while the total cost decreases rapidly between 55% and 20%. When $\alpha = 60\%$, the operational status of thermal units in both ends are shown in Figure 5, where "o" indicates motion while "$*$" indicates idleness. The dispatching results for the sending and receiving ends are shown in Figs. 6 and 7 (the specific strategies are shown in Tables A.I and A.II in the Appendix). The above results provide a reference for decision makers to reasonably select the confidence probability, while considering the conservativeness of the system and improving its economy.

TABLE 5. Comparison results for different confidence probabilities.

Spatial constrained parameters				Cost ($)				The probability of cross-boundary	
α	r_W	$r^A{}_L$	$r^B{}_L$	Total	Thermal	Spinning Reserve	Flexible load	Area A	Area B
60%	28.5	19.2	28.5	2.24e7	4.22e6	1.62e7	2.01e6	0.0101%	0.0001%
55.5%	26.4	17.6	26.4	2.11e7	4.18e6	1.50e7	1.98e6	0.0442%	0.0009%
45%	21.7	14.0	21.7	1.80e7	3.98e6	1.22e7	1.87e06	0.7840%	0.0390%
30%	14.5	9.7	14.5	1.36e7	3.67e6	8.23e6	1.73e6	12.8088%	3.0072%
20%	8.9	5.9	8.9	1.08e7	4.11e6	5.03e6	1.62e6	79.7808%	26.7091%
10%	0.89	0.59	0.89	9.82e6	3.89e6	5.03e5	1.54e6	100.0000%	98.6885%

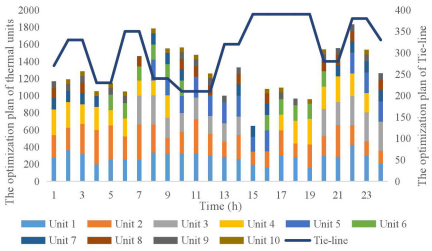

FIGURE 6. Operational strategy of sending end.

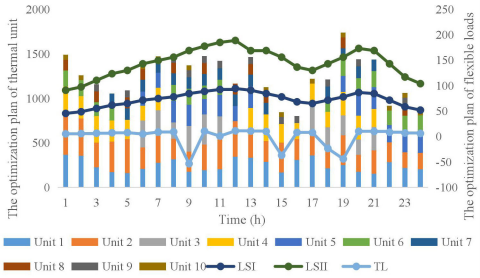

FIGURE 7. Operational strategy of receiver system.

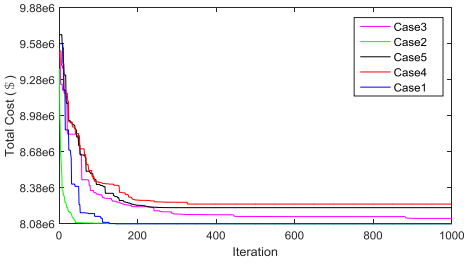

FIGURE 8. Convergence of different algorithm combinations.

To further illustrate the competitiveness of HEFO compared with other algorithms, Table 6 shows the scheduling results of the filter coordination algorithm combined with different algorithms when $\alpha = 0.6$. The convergence of the algorithm is shown in Fig. 8. (Case 1: IMFO + DE + GA; Case 2: MFO + DE + GA; Case 3: Particle swarm optimization (PSO) + DE + GA; Case 4: DE + DE + GA; Case 5: GA + DE + GA)

It can be seen from the results in Table 6 that the combination algorithm we selected has obtained the most satisfactory results. Simultaneously, it is proved that the improved Moth-flame Optimization has the advantages of faster convergence

TABLE 6. Comparison of different algorithms.

	Cost($)			
	Total	Thermal	Rotating reserve	Flexible scheduling
Case1	8.08e6	3.74e6	4.05e6	2.88e5
Case2	8.10e6	3.74e6	4.07e6	2.91e5
Case3	8.14e6	3.79e6	4.05e6	2.97e5
Case4	8.30e6	3.88e6	4.12e6	2.97e5
Case5	8.28e6	3.90e6	4.09e6	2.94e5

speed and higher accuracy in solving continuous variables, and has obvious advantages in dealing with optimization problems with complex constraints. It can be seen from Fig. 8. that the combination algorithm selected in this paper also has certain advantages in convergence speed.

2) EFFECTS OF SPATIAL CONSTRAINT PARAMETERS

We studied the effect of different spatial constraint parameters on scheduling results. The wind farms and loads were divided into several parts with the same total power, while the prediction accuracy was maintained at 68.27%. The total costs under different confidence probabilities are in shown in Fig. 9. (Case 1: 2 wind generators and 2 loads; Case 2: 10 wind turbines and 10 loads; Case 3: 20 wind turbines and 10 loads; Case 4: 20 wind turbines and 20 loads; Case 5: 30 wind turbines and 30).

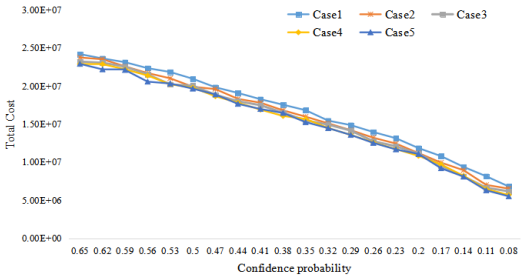

FIGURE 9. Impact of spatial cluster effect on cost (prediction accuracy = 68.27%).

It can be seen from Fig. 9 that with increase in the number of wind farms and loads, the distribution of wind turbines and loads become sparser, the spatial constraints parame-

ters increase, so the volatility of uncertain variables can be described more carefully while the dispatching cost gradually reduces. Thus, better dispatching results and operation schemes are obtained.

3) ECONOMIC AND CONSERVATIVE DECISION MAKING

In order to balance economy and conservatism operational strategies, it is important to scientifically and reasonably select the confidence probability of uncertain sets. We explored the dispatching cost and the probability of constraint violation for interconnected systems under different confidence probabilities. We set the prediction accuracy of both source and loads to 68.27% and the number of wind generators and loads in A / B to 10. A comparison of results under different confidence probabilities is shown in Fig. 10.

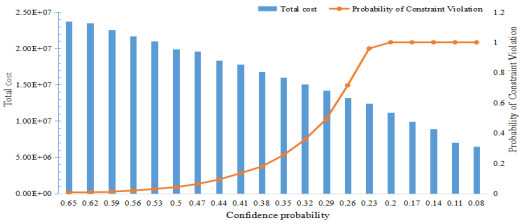

FIGURE 10. System economy and conservatism under different confidence probabilities in case 1.

Fig. 10 shows that the probability of violation for system constraints increases nonlinearly with the confidence probability. The constraint violation probability increases rapidly when α is between [23%, 50%]. When $\alpha > 23\%$, the violation probability is approximately 1 and unchanged, while it increases slowly and is below 3% when $\alpha < 50\%$.

B. CASE2: HAMI POWER GRID IN XINJIANG

In order to verify the economy and conservativeness of the robust optimal dispatching model with uncertainties on both source and load sides in actual power system dispatching problems, the sending end was replaced by the Hami power grid in Xinjiang. The Hami regional power grid is centered on Hami city and forms a grid with +800 KV, 750 KV, and 220 KV voltage levels as the backbone. The grid structure and line parameters are shown in Fig. 11. The No. 1 and 2 wind farm groups consist of 10 and 12 wind farms with total capacities of 2000 MW and 1000 MW, and the matching DC thermal plants have 8 units with a rated output of 4800 MW. The forecasting of loads at both ends and wind power output are shown in Fig. 12. We set the number of loads on both ends at 30. The operating parameters of the thermal units on the sending side and the tie-line are listed in Table 7-9. The receiving end is still equivalent to the IEEE-39 bus system and the unit operation parameters are the same as those of Case 1.

The penalty coefficient, the controllable load and the algorithm parameters of the system were also unchanged.

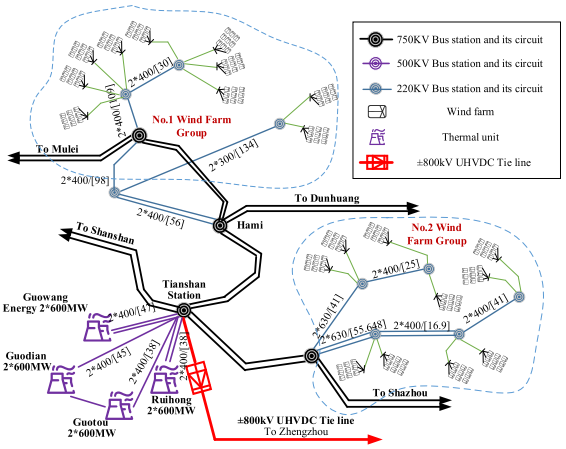

FIGURE 11. Structure and line parameters of Hami power grid.

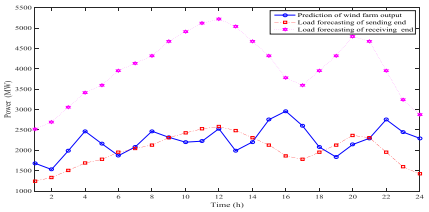

FIGURE 12. Forecast values of wind power output and loads.

TABLE 7. Fuel cost coefficients of thermal units at sending end.

a_i	b_i	c_i	d_i	e_i
786.7988	38.5379	0.1524	450	0.041

TABLE 8. Operating parameters of thermal units at sending end.

NO.	Upper	Lower	Minimum stop-start time(h)	Climbing (MW/h)	stop-start cost (MW/ $)
Unit 1-6	600	200	8	200	20000

TABLE 9. Operating parameters of tie-line.

Minimum maintenanc e time(h)	Climbing (MW)	Upper (MW)	Lower(MW)
4	150	2000	400

Fig. 13 shows the dispatching cost and the probability of constraint violation for interconnected systems under different confidence probabilities. The results are similar to those shown in Fig. 10 in Case 1. The system dispatcher can balance economy and conservatism of the system consistently and reasonably, and obtain the corresponding operation scheme based on the non-linear relationship between the confidence probability, system cost and constraint violation probability. When the confidence probability is reduced to 0.44, the total

TABLE 10. Operation strategy of sender system.

Time	MW								
	Unit 1	Unit 2	Unit 3	Unit 4	Unit 5	Unit 6	Unit 7	Unit 8	Tie-line
1	-	360.36	-	412.87	269.18	-	515.59	-	1750
2	-	406.63	-	524.76	417.81	-	458.75	-	1870
3	-	462.58	-	334.70	478.41	-	397.50	-	1870
4	-	378.48	-	522.30	368.38	-	291.56	-	1920
5	-	455.29	-	411.45	467.29	-	466.91	-	1920
6	-	478.46	-	318.41	456.68	-	544.37	-	1830
7	-	416.87	-	487.19	466.16	-	485.93	-	1830
8	-	494.84	-	330.80	346.46	-	582.35	-	1970
9	284.24	-	-	461.21	389.32	347.41	446.45	417.82	1970
10	440.67	-	457.64	314.36	414.32	233.66	-	551.11	1960
11	390.91	-	552.64	490.86	-	354.06	-	438.47	1960
12	569.52	-	366.98	361.74	-	514.40	-	362.59	1830
13	455.97	-	445.31	-	-	423.16	-	445.57	1830
14	470.53	-	589.06	-	-	336.80	-	490.85	1910
15	384.54	-	486.85	-	-	441.85	-	369.18	1910
16	356.63	-	407.11	-	-	241.88	-	363.81	1990
17	313.83	513.09	387.02	-	-	348.88	-	-	1990
18	461.16	450.98	409.57	-	-	-	494.62	-	1890
19	429.13	392.27	495.51	-	414.65	-	500.14	-	1890
20	-	377.96	471.05	-	584.09	-	370.63	-	1850
21	-	451.32	550.36	-	450.92	-	444.83	-	1850
22	-	411.10	430.01	-	457.53	-	415.44	-	1990
23	-	427.31	336.46	480.03	258.94	-	233.95	-	1990
24	-	297.99	305.01	281.40	411.91	-	347.01	-	1990

"-" represents that the thermal unit is in shutdown state.

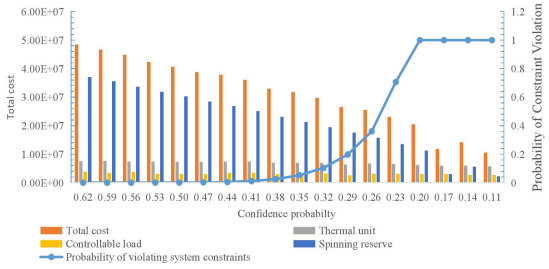

FIGURE 13. System economy and conservatism under different confidence probabilities in Case 2.

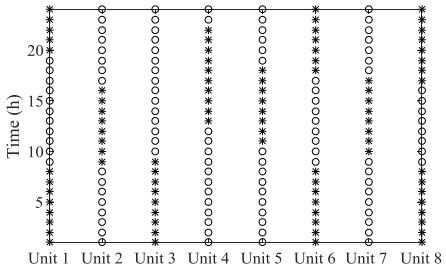

FIGURE 14. Operation status of thermal units at sending end.

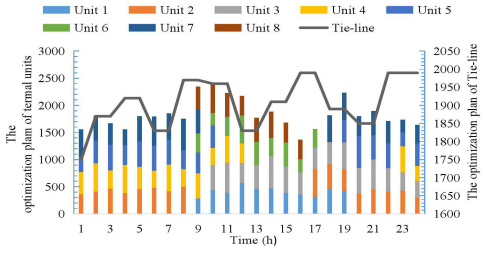

FIGURE 15. The optimization plan of thermal units and tie-line.

cost of the system decreases by 21.9% compared with that of $\alpha = 0.62$, while the probability of system constraint violation remains at a low level of only 0.5%. Fig. 14 shows the operation status of thermal units for $\alpha = 0.44$ at the sending end, where "o" denotes operation while "∗"corresponds to idleness. The detailed dispatching plan is shown in Fig. 15, and the output power of each unit and tie-line are shown in Table 10.

From the above results, it can be seen that the proposed robust optimal dispatching model for CRIG is effective in practical power grids. In practical problems, a more detailed and comprehensive analysis of the impact of the confidence probability on dispatching results and the security of the system should be undertaken. Considering the actual prediction accuracy of uncertain variables, the appropriate confidence probability must be selected from within the acceptable probability range of the system exceeding safety constraints, that the robustness and economy of the system are both taken into account.

TABLE 11. Operation strategy of sender system.

Time	MW										
	Unit 1	Unit 2	Unit 3	Unit 4	Unit 5	Unit 6	Unit 7	Unit 8	Unit 9	Unit 10	Tie-line
1	273.53	264.21	-	300.00	-	-	130.00	120.00	80.00	-	270
2	360.45	264.36	-	300.00	-	-	130.00	-	80.00	55.00	330
3	314.85	352.65	-	231.20	-	-	130.00	120.00	80.00	55.00	330
4	194.84	403.88	-	268.15	-	-	130.00	-	-	55.00	230
5	251.58	399.33	-	178.15	-	180.00	-	-	80.00	55.00	230
6	254.15	269.21	-	210.55	-	180.00	-	-	80.00	55.00	350
7	249.83	410.21	340.00	174.56	-	164.97	-	120.00	-	-	350
8	336.06	327.05	340.00	171.61	243.00	180.00	130.00	-	-	55.00	240
9	317.96	186.05	238.00	261.61	182.86	180.00	130.00	-	-	55.00	240
10	318.95	256.48	220.17	-	200.86	180.00	130.00	120.00	80.00	55.00	210
11	324.05	397.48	257.01	-	243.00	-	-	120.00	80.00	55.00	210
12	297.18	256.48	207.56	-	243.00	-	-	120.00	80.00	55.00	210
13	284.96	178.45	213.97	-	243.00	-	-	-	80.00	-	320
14	259.04	283.16	213.89	-	243.00	-	130.00	120.00	80.00	-	320
15	192.75	155.25	-	-	170.00	-	130.00	-	-	-	390
16	161.69	189.63	-	-	243.00	180.00	130.00	120.00	-	55.00	390
17	302.69	293.01	-	182.07	-	180.00	-	-	80.00	55.00	390
18	275.43	164.26	-	267.13	-	180.00	-	-	80.00	-	390
19	153.57	275.68	-	300.00	-	174.97	-	-	-	55.00	390
20	294.57	233.21	313.81	262.90	-	180.00	-	120.00	80.00	55.00	280
21	285.09	369.75	270.33	300.00	-	-	130.00	120.00	80.00	-	280
22	426.09	228.75	340.00	264.77	243.00	-	130.00	120.00	80.00	-	380
23	301.06	164.83	340.00	222.15	243.00	-	130.00	-	80.00	55.00	380
24	205.97	150.33	340.00	-	236.00	-	130.00	120.00	80.00	-	330

"-" represents that the thermal unit is in shutdown state.

TABLE 12. Operation strategy of receiver system.

Time	Thermal(MW)										Flexible loads (MW)		
	Unit 1	Unit 2	Unit 3	Unit 4	Unit 5	Unit 6	Unit 7	Unit 8	Unit 9	Unit 10	LSI	LSII	TL
1	363.89	469.75	-	300.00	-	180.00	-	120.00	-	55.00	45.50	91.01	5.42
2	355.94	417.41	-	251.63	-	180.00	-	-	-	55.00	48.76	97.51	5.81
3	226.27	276.41	-	300.00	-	155.16	-	120.00	80.00	-	55.26	110.51	6.58
4	170.32	341.45	-	238.07	-	172.89	130.00	-	-	-	61.76	123.51	7.36
5	159.84	380.98	-	218.37	-	-	130.00	120.00	80.00	-	65.01	130.01	7.74
6	208.52	239.98	302.37	164.66	161.37	-	130.00	120.00	-	55.00	71.51	143.01	4.97
7	277.15	301.79	285.90	254.66	167.58	-	130.00	-	-	55.00	74.76	149.52	8.90
8	314.30	232.17	183.90	-	240.58	180.00	130.00	120.00	80.00	-	78.01	156.02	9.29
9	173.30	229.10	285.90	-	237.67	180.00	130.00	-	80.00	55.00	84.51	169.02	-53.35
10	194.23	285.27	340.00	-	173.92	150.86	130.00	120.00	80.00	-	88.81	177.63	10.58
11	202.52	355.59	238.00	-	243.00	170.26	130.00	-	80.00	-	92.50	185.01	0.86
12	343.52	400.65	-	-	170.00	-	130.00	120.00	-	-	94.44	188.87	11.25
13	332.89	259.65	-	300.00	243.00	-	130.00	120.00	80.00	-	91.01	168.84	10.84
14	286.22	233.75	-	300.00	-	-	130.00	120.00	-	55.00	84.51	169.02	10.06
15	165.76	335.69	-	210.00	-	-	-	-	80.00	55.00	78.01	156.02	-36.87
16	306.76	234.24	-	180.88	-	-	-	-	80.00	-	68.26	136.51	8.13
17	356.76	287.95	281.92	236.97	-	-	-	-	-	55.00	65.01	130.01	7.74
18	215.76	229.45	230.66	174.17	-	152.50	130.00	-	80.00	-	71.51	143.01	-23.44
19	251.90	332.86	223.97	264.17	179.63	180.00	130.00	120.00	-	55.00	78.01	156.02	-43.94
20	174.76	191.86	171.83	266.84	243.00	180.00	130.00	-	80.00	-	86.62	173.23	10.32
21	153.22	262.34	262.94	202.93	243.00	180.00	130.00	-	-	-	84.51	169.02	10.06
22	284.33	223.07	-	-	194.25	161.58	-	-	-	55.00	71.51	143.01	8.52
23	219.36	174.06	-	-	243.00	169.92	-	120.00	80.00	55.00	58.51	117.01	6.97
24	203.42	184.24	-	-	242.74	180.00	-	-	-	55.00	52.01	104.01	6.19

"-" represents that the thermal unit is in shutdown state.

VI. CONCLUSION

We propose a robust optimal scheduling model considering the bilateral uncertainties of source and load for interconnected systems with large-scale grid connected RES. Spatial constraints are introduced to flexibly adjust the boundaries of uncertain sets by varying the confidence

probability to balance economy and conservatism. According to the characteristics of the model, a filter-based co-evolutionary algorithm is proposed. The proposed algorithm solves the mixed-integer non-convex non-linear programming model effectively. Furthermore, we analyze the effects of prediction accuracy constraints, confidence probability and spatial cluster on dispatching cost and constraint violation. The results provide reference for the reasonable selection of the confidence probability while considering the system conservativeness and improving the economy. Finally, the feasibility and validity of the proposed model and algorithm in the actual power grid are demonstrated taking the Hami power grid in Xinjiang as a case study.

APPENDIX

See Table 11 and 12 here.

REFERENCES

[1] J. Hui, W. Cai, C. Wang, and M. Ye, "Analyzing the penetration barriers of clean generation technologies in China's power sector using a multi-region optimization model," *Appl. Energy*, vol. 185, pp. 1809–1820, Jan. 2017, doi: 10.1016/j.apenergy.2016.02.034.

[2] Y. Nie, G. Zhang, and H. Duan, "An interconnected panorama of future cross-regional power grid: A complex network approach," *Resour. Policy*, vol. 67, Aug. 2020, Art. no. 101692, doi: 10.1016/j.resourpol.2020.101692.

[3] Y. Ding, C. Shao, J. Yan, Y. Song, C. Zhang, and C. Guo, "Economical flexibility options for integrating fluctuating wind energy in power systems: The case of China," *Appl. Energy*, vol. 228, pp. 426–436, Oct. 2018, doi: 10.1016/j.apenergy.2018.06.066.

[4] F. Zeng, G. Li, Z. Bie, H. Cheng, Y. Zheng, and J. Geng, "Decentralized dispatch method for multi-area interconnected power systems considering cross-area tie-line transaction strategy," *Autom. Electr. Power Syst.*, vol. 42, no. 16, pp. 32–40, 2018.

[5] C. Wang, J. Zhu, Y. Xia, Y. Guo, X. Mo, and T. Luo, "A real-time decentralized robust dispatch approach of multi-area power system," *Power Syst. Technol.*, vol. 43, pp. 4478–4485, Dec. 2019.

[6] K. Lyu, H. Tang, K. Wang, B. Tang, and H. Wu, "Coordinated dispatching of source-grid-load for inter-regional power grid considering uncertainties of both source and load sides," *Autom. Electr. Power Syst.*, vol. 43, no. 22, pp. 38–45, 2019.

[7] H. Sun, J. Meng, and C. Peng, "Coordinated optimization scheduling of multi-region virtual power plant with wind-power/photovoltaic/hydropower/carbon-capture units," *Power Syst. Technol.*, vol. 43, pp. 4040–4051, Jul. 2019.

[8] B. Zhao, H. Qiu, R. Qin, X. Zhang, W. Gu, and C. Wang, "Robust optimal dispatch of AC/DC hybrid microgrids considering generation and load uncertainties and energy storage loss," *IEEE Trans. Power Syst.*, vol. 33, no. 6, pp. 5945–5957, Nov. 2018, doi: 10.1109/TPWRS.2018.2835464.

[9] X. Zhang, C. Zhao, J. Liang, K. Li, and J. Zhong, "Robust fuzzy scheduling of power systems considering bilateral uncertainties of generation and demand side," *Autom. Electr. Power Syst.*, vol. 42, no. 17, pp. 67–75, 2018.

[10] X. Ge, G. Hao, S. Xia, and Y. Fu, "An optimal system scheduling method with high proportion of wind power," *Power Syst. Technol.*, vol. 43, pp. 390–399, 2019.

[11] E. Jafari, S. Soleymani, B. Mozafari, and T. Amraee, "Optimal operation of a micro-grid containing energy resources and demand response program," *Int. J. Environ. Sci. Technol.*, vol. 15, no. 10, pp. 2169–2182, Oct. 2018, doi: 10.1007/s13762-017-1525-6.

[12] V. A. Evangelopoulos, I. I. Avramidis, and P. S. Georgilakis, "Flexibility services management under uncertainties for power distribution systems: Stochastic scheduling and predictive real-time dispatch," *IEEE Access*, vol. 8, pp. 38855–38871, 2020, doi: 10.1109/ACCESS.2020.2975663.

[13] D. Liu, Y. Wang, and Y. Shen, "Electric vehicle charging and discharging coordination on distribution network using multi-objective particle swarm optimization and fuzzy decision making," *Energies*, vol. 9, no. 3, p. 186, Mar. 2016, doi: 10.3390/en9030186.

[14] M. McPherson and B. Karney, "A scenario based approach to designing electricity grids with high variable renewable energy penetrations in Ontario, Canada: Development and application of the SILVER model," *Energy*, vol. 138, pp. 185–196, Nov. 2017, doi: 10.1016/j.energy.2017.07.027.

[15] X. Ma, Y. Jin, and Q. Dong, "A generalized dynamic fuzzy neural network based on singular spectrum analysis optimized by brain storm optimization for short-term wind speed forecasting," *Appl. Soft Comput.*, vol. 54, pp. 296–312, May 2017, doi: 10.1016/j.asoc.2017.01.033.

[16] S. Barik and D. Das, "Impact of FFC distributed generations in a DNR in the presence of renewable and load uncertainties by mixed-discrete particle swarm-based point estimation method," *IET Renew. Power Gener.*, vol. 13, no. 9, pp. 1431–1445, Jul. 2019, doi: 10.1049/iet-rpg.2018.5834.

[17] C. Wang, Z. Wang, J. Wang, and Y. Hou, "Chance-constrained maintenance scheduling for interdependent power and natural gas grids considering wind power uncertainty," *IET Gener., Transmiss. Distrib.*, vol. 13, no. 5, pp. 686–694, Mar. 2019, doi: 10.1049/iet-gtd.2018.5887.

[18] D. Lianjie, C. Degang, W. Ningling, and L. Zhanhui, "Key energy-consumption feature selection of thermal power systems based on robust attribute reduction with rough sets," *Inf. Sci.*, vol. 532, pp. 61–71, Sep. 2020, doi: 10.1016/j.ins.2020.03.085.

[19] P. Li, D. Yu, M. Yang, and J. Wang, "Flexible look-ahead dispatch realized by robust optimization considering CVaR of wind power," *IEEE Trans. Power Syst.*, vol. 33, no. 5, pp. 5330–5340, Sep. 2018, doi: 10.1109/TPWRS.2018.2809431.

[20] J. Zhao, T. Zheng, and E. Litvinov, "A unified framework for defining and measuring flexibility in power system," *IEEE Trans. Power Syst.*, vol. 31, no. 1, pp. 339–347, Jan. 2016, doi: 10.1109/TPWRS.2015.2390038.

[21] R. Torabi, A. Gomes, D. Lobo, and F. Morgado-Dias, "Modelling demand flexibility and energy storage to support increased penetration of renewable energy resources on Porto Santo," *Greenhouse Gases, Sci. Technol.*, Jun. 2020, doi: 10.1002/ghg.2005.

[22] Y. Li, C. Wang, G. Li, J. Wang, D. Zhao, and C. Chen, "Improving operational flexibility of integrated energy system with uncertain renewable generations considering thermal inertia of buildings," *Energy Convers. Manage.*, vol. 207, Mar. 2020, Art. no. 112526, doi: 10.1016/j.enconman.2020.112526.

[23] N. Yoshioka, H. Asano, and S. Bando, "Economic evaluation of charging/discharging control of electric vehicles as system flexibility considering control participation rate," *Electr. Eng. Jpn.*, vol. 211, nos. 1–4, pp. 15–25, Jun. 2020, doi: 10.1002/eej.23267.

[24] E. Nycander, L. Söder, J. Olauson, and R. Eriksson, "Curtailment analysis for the nordic power system considering transmission capacity, inertia limits and generation flexibility," *Renew. Energy*, vol. 152, pp. 942–960, Jun. 2020, doi: 10.1016/j.renene.2020.01.059.

[25] S. Zhai, H. Zhou, Z. Wang, and G. He, "Analysis of dynamic appliance flexibility considering user behavior via non-intrusive load monitoring and deep user modeling," *CSEE J. Power Energy Syst.*, vol. 6, no. 1, pp. 41–51, 2020, doi: 10.17775/CSEEJPES.2019.02100.

[26] D. A. Tejada-Arango, G. Morales-Espana, S. Wogrin, and E. Centeno, "Power-based generation expansion planning for flexibility requirements," *IEEE Trans. Power Syst.*, vol. 35, no. 3, pp. 2012–2023, May 2020, doi: 10.1109/TPWRS.2019.2940286.

[27] A. Turk, Q. Wu, M. Zhang, and J. Østergaard, "Day-ahead stochastic scheduling of integrated multi-energy system for flexibility synergy and uncertainty balancing," *Energy*, vol. 196, Apr. 2020, Art. no. 117130, doi: 10.1016/j.energy.2020.117130.

[28] G. Mohy-Ud-Din, K. M. Muttaqi, and D. Sutanto, "Transactive energy-based planning framework for VPPs in a co-optimised day-ahead and real-time energy market with ancillary services," *IET Gener., Transmiss. Distrib.*, vol. 13, no. 11, pp. 2024–2035, Jun. 2019, doi: 10.1049/iet-gtd.2018.5831.

[29] A. Dadkhah, B. Vahidi, M. Shafie-Khah, and J. P. S. Catalão, "Power system flexibility improvement with a focus on demand response and wind power variability," *IET Renew. Power Gener.*, vol. 14, no. 6, pp. 1095–1103, Apr. 2020, doi: 10.1049/iet-rpg.2019.0123.

[30] M. I. Azim, W. Tushar, and T. K. Saha, "Investigating the impact of P2P trading on power losses in grid-connected networks with prosumers," *Appl. Energy*, vol. 263, Apr. 2020, Art. no. 114687, doi: 10.1016/j.apenergy.2020.114687.

[31] C. Huang, C. Wang, N. Xie, and Y. Wang, "Robust coordination expansion planning for active distribution network in deregulated retail power market," *IEEE Trans. Smart Grid*, vol. 11, no. 2, pp. 1476–1488, Mar. 2020, doi: 10.1109/TSG.2019.2938723.

[32] G. Xiong and D. Shi, "Hybrid biogeography-based optimization with brain storm optimization for non-convex dynamic economic dispatch with valve-point effects," *Energy*, vol. 157, pp. 424–435, Aug. 2018, doi: 10.1016/j.energy.2018.05.180.
[33] H. Narimani, S.-E. Razavi, A. Azizivahed, E. Naderi, M. Fathi, M. H. Ataei, and M. R. Narimani, "A multi-objective framework for multi-area economic emission dispatch," *Energy*, vol. 154, pp. 126–142, Jul. 2018, doi: 10.1016/j.energy.2018.04.080.
[34] X. Shen, D. Zou, N. Duan, and Q. Zhang, "An efficient fitness-based differential evolution algorithm and a constraint handling technique for dynamic economic emission dispatch," *Energy*, vol. 186, Nov. 2019, Art. no. 115801, doi: 10.1016/j.energy.2019.07.131.
[35] M. Basu, "Squirrel search algorithm for multi-region combined heat and power economic dispatch incorporating renewable energy sources," *Energy*, vol. 182, pp. 296–305, Sep. 2019, doi: 10.1016/j.energy.2019.06.087.
[36] X. Li, W. Wang, H. Wang, J. Wu, X. Fan, and Q. Xu, "Dynamic environmental economic dispatch of hybrid renewable energy systems based on tradable green certificates," *Energy*, vol. 193, no. 116699, pp. 775–792, 2020, doi: 10.1016/j.energy.2019.116699.
[37] Z. Zhu and J. Wang, "Dynamic economic emission dispatch based on modified NSGA-II forpower system," *Electr. Power Autom. Equip.*, vol. 37, no. 2, pp. 176–183, 2017.
[38] D. C. Walters and G. B. Sheble, "Genetic algorithm solution of economic dispatch with valve point loading," *IEEE Trans. Power Syst.*, vol. 8, no. 3, pp. 1325–1332, Aug. 1993, doi: 10.1109/59.260861.
[39] N. I. M. Gould, Y. Loh, and D. P. Robinson, "A nonmonotone filter SQP method: Local convergence and numerical results," *SIAM J. Optim.*, vol. 25, no. 3, pp. 1885–1911, Jan. 2015, doi: 10.1137/140996677.
[40] S. Mirjalili, "Moth-flame optimization algorithm: A novel nature-inspired heuristic paradigm," *Knowl.-Based Syst.*, vol. 89, pp. 228–249, Nov. 2015, doi: 10.1016/j.knosys.2015.07.006.

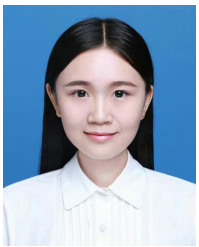

XIAOZHU LI received the B.E. degree in measurement and control technology and instruments from the Changsha University of Technology, in 2013, and the M.E. degree in control science and control engineering from Xinjiang University, China, in 2017, where she is currently pursuing the Ph.D. degree with the Department of Electrical Engineering. Her research interests include power system non-linear control and stability analysis, power system adaptive control, robust control, and dynamic environmental economic dispatch.

WEIQING WANG is currently a Professor with the Department of Electrical Engineering, Xinjiang University. He is also a Ph.D. Supervisor. His research interests include development of key components of large-scale wind turbine, intelligent control and detection of the whole machine, relay protection, and grid-connected transmission technology.

HAIYUN WANG is currently a Professor with the Department of Electrical Engineering, Xinjiang University. She is also a Deputy Secretary with the New Energy Industry Innovation Alliance. Her research interests include key components of large-wind turbine, detection technology of wind turbines, and power system security and stability and its control and protection.

JIAHUI WU received the B.E. degree in control engineering from the Beijing University of Chemical Technology, in 2011, and the M.E. degree in electrical engineering from Xinjiang University, China, in 2015. She is currently a Lecturer with the Department of Electrical Engineering, Xinjiang University. Her research interests include power system stability and integration of the renewable resources.

QIDAN XU received the M.E. degree in electrical engineering from Xinjiang University, China, in 2017. He is currently a Fellow with State Grid Xinjiang Electric Power Company Ltd. He is also with State Grid Economic and Technological Research Institute. His research interests include power system and its automation and power engineering cost analysis.